A&A 428, 227–233 (2004)
DOI: 10.1051/0004-6361:20041071

Astronomy & Astrophysics

Dynamics of circularly polarised Alfvén waves in a stratified medium

R. Turkmani⋆ and U. Torkelsson

Chalmers University of Technology/Göteborg University, Department of Astronomy & Astrophysics, 412 96 Gothenburg, Sweden
e-mail: r.turkmani@ic.ac.uk

Received 10 April 2004 / Accepted 9 August 2004

Abstract. We present a numerical study of the propagation of circularly polarised Alfvén waves in a plane-parallel stratified medium. Because of the stratification there is a global gradient in the magnetic pressure of the wave, which accelerates the plasma and supports it against gravity. The spatial distribution of the wave force is determined by the amplitude of the Alfvén wave which in its turn is set by the influences of dissipation, reflection and parametric decay on the wave. The Alfvén wave is partially reflected off the smooth density gradient. The relative amplitude of the reflected wave is proportional to the background magnetic field strength and is independent of the absolute amplitude of the wave. At high amplitudes strong backward propagating Alfvén waves are generated through the parametric decay of the Alfvén wave, and by reflection off density fluctuations generated by the wave front.

Key words. magnetohydrodynamics (MHD) – waves – Sun: solar wind – stars : mass-loss

1. Introduction

Alfvén waves are one of the most common magnetohydrodynamic (MHD) phenomena; they were first observed in the solar wind over 30 years ago (e.g., Belcher & Davis 1971). At that time they had already been considered theoretically as a way to transmit energy from the photosphere to the corona and solar wind because they do not easily dissipate. The theoretical problem of the behaviour of Alfvén waves in the solar atmosphere has been investigated by Biermann (1948) and Ferraro (1954).

The purpose of this paper is to investigate the propagation of a circularly polarised Alfvén wave in a stratified medium. In most of the studies of the propagation of Alfvén waves in the solar atmosphere a linearly polarised Alfvén wave has been assumed (e.g., Boynton & Torkelsson 1996; Ofman & Davila 1997; Nakariakov et al. 2000). The polarisation is important because it determines the profile of the magnetic pressure inside the Alfvén wave. Linearly polarised Alfvén waves are compressible to the second order because the magnetic pressure, $B_\perp^2/2\mu_0$, is modulated on half the wave length of the Alfvén wave itself (Alfvén & Fälthammar 1963) and therefore they steepen and form current sheets at the nodes of the fluctuating magnetic field (e.g., Cohen & Kulsrud 1974; Boynton & Torkelsson 1996) In a circularly polarised Alfvén wave, the magnetic pressure is constant along the wave, which is the physical reason why it is an exact solution of the non-linear MHD equations. However the Alfvén wave is still subject to a parametric instability (Galeev & Oraevskii 1963; Sagdeev & Galeev 1969). In the presence of a density fluctuation, a circularly polarised Alfvén wave couples to a forward propagating density wave and a backward propagating magnetic wave, none of which is necessarily a normal mode of the plasma. Parametric decay has received attention for its potential to generate backward propagating waves even in areas with smooth density variations like the polar solar wind (e.g., Sagdeev & Galeev 1969; Del Zanna et al. 2001).

In a previous paper (Turkmani & Torkelsson 2003) we studied Alfvén waves propagating through a homogeneous medium. We found then that the parametric decay was the most important non-linear effect affecting the Alfvén waves in a strongly magnetised medium. In a weakly magnetised medium a backward propagating wave is rather generated by reflection at the Alfvén wave front. By introducing stratification the relative strength of the background magnetic field will vary with the vertical coordinate. Thus we can expect different physical mechanisms to act on different parts of the wave at the same time, but these regions are coupled together through the different wave modes.

A seemingly trivial effect of the stratification is that the amplitude and wave length of the Alfvén wave depends on its position. One important consequence of this is that the magnetic pressure of the wave decreases as we move upwards, which introduces a magnetic pressure gradient that can support the plasma against the gravity or drive an outflow. Another

⋆ *Present address:* Space and Atmospheric Physics, The Blackett Laboratory, Imperial College, London, UK.

consequence of the stratification is that the Alfvén speed increases with height. The wave length will therefore increase and may even exceed the density scale height, which means that the WKB approximation does not apply. Under these circuumstances there will be a continuous partial reflection of the wave off the smooth gradient in the background density (e.g., Leroy 1980; Leer et al. 1982; An et al. 1989; Oughton et al. 2001; Lou & Rosner 1994). In particular An et al. (1989) find that with an exponential stratification the wave is reflected completely since it reaches infinity in a finite time and is therefore effectively trapped between the source and infinity.

For simplicity, we will limit ourselves in this paper to a one-dimensional model that we solve numerically. Apart from limiting the computational demands it also allows us to concentrate on a few physical effects during the analysis of our simulations, and exclude complicated mechanisms such as phase mixing or the coupling of the Alfvén wave to waves that are propagating at an angle to the background magnetic field. The equations that we solve and the basic properties of the initial states of our models are described in Sect. 2. The results of our simulations are presented in Sect. 3, and are then further discussed in Sect. 4.

2. Mathematical formulation

The basic equations describing the dynamics of Alfvén waves in a gravitationally stratified isothermal medium are the MHD-equations:

$$\frac{\partial \rho}{\partial t} + \nabla \cdot (\rho \boldsymbol{v}) = 0, \tag{1}$$

$$\frac{\partial (\rho \boldsymbol{v})}{\partial t} + \nabla \cdot (\boldsymbol{v} \rho \boldsymbol{v}) = -\nabla p + \boldsymbol{J} \times \boldsymbol{B} + \rho \boldsymbol{g}, \tag{2}$$

$$\frac{\partial \boldsymbol{B}}{\partial t} = \nabla \times (\boldsymbol{v} \times \boldsymbol{B} - \eta \nabla \times \boldsymbol{B}), \tag{3}$$

and the magnetic field $\boldsymbol{B}$ fulfills

$$\nabla \cdot \boldsymbol{B} = 0. \tag{4}$$

Here ρ is the density, $\boldsymbol{v}$ the velocity, $\boldsymbol{J} = \nabla \times \boldsymbol{B}/\mu_0$ the current density, μ_0 the magnetic permeability of free space, $\boldsymbol{g}$ the gravitational acceleration, and η the magnetic diffusivity, which is negligible. p is taken to be the pressure of fully ionised hydrogen. Eqs. (1), and (2) express the conservation of mass and momentum, respectively, and Eq. (3) is the induction equation. The constraint (4) is fulfilled by Eq. (3), if it is imposed as an initial condition.

The gravitational field in our simulations is given by

$$\boldsymbol{g} = -\frac{GM}{(R+z)^2}\hat{\boldsymbol{z}}, \tag{5}$$

where G is the gravitational constant, M the mass of the sun, R the radius of the sun and z the height above the solar surface. The density is taken to be $5 \times 10^{-13}\,\mathrm{kg\,m^{-3}}$ at the bottom of the corona and varies with z as

$$\rho_0(z) = \rho_0(0) \exp\left(-\frac{R}{H}\frac{z}{R+z}\right), \tag{6}$$

where $H = 2k_\mathrm{B}TR^2/(GMm_\mathrm{H})$ is the scale height at $z = 0$, k_B Boltzmann's constant, T the temperature and m_H the mass of the hydrogen atom.

The isothermal density distribution can be viewed as the result of the high thermal conductivity of the plasma in the solar corona. The role of thermal conduction in the dynamic equations is more complicated though. While thermal conduction in general damps any compressive wave (e.g., De Moortel & Hood 2004) the isothermal MHD-equations do not possess this property. Rather these equations have a solution describing an undamped acoustic wave with a speed

$$c_\mathrm{s} = \sqrt{\frac{p_0}{\rho_0}}, \tag{7}$$

where p_0 is the background pressure. This wave is slower than the adiabatic sound wave by a factor $\sqrt{\gamma}$, thus suggesting that the difference between isothermal and adiabatic compressive waves is quantitative rather than qualitative.

Alfvén waves on the other hand are to lowest order incompressible and therefore insensitive to the thermodynamics. Within the WKB-approximation a circularly polarised forward propagating Alfvén wave in a stratified medium with a background magnetic field $\boldsymbol{B} = B_0\hat{\boldsymbol{z}}$ is described by the transverse magnetic field

$$\boldsymbol{B}_\perp(z) = B_\perp(z)[\cos(k(z)\,z - \omega t)\hat{\boldsymbol{x}} + \sin(k(z)\,z - \omega t)\hat{\boldsymbol{y}}], \tag{8}$$

and the velocity

$$\boldsymbol{v}_\perp = -\frac{\boldsymbol{B}_\perp}{\sqrt{\mu_0 \rho_0}}. \tag{9}$$

The wave obeys the dispersion relation

$$\omega = v_\mathrm{A}(z)\,k(z) \tag{10}$$

with the Alfvén velocity

$$v_\mathrm{A}(z) = \frac{B_0}{\sqrt{\mu_0 \rho_0(z)}}. \tag{11}$$

Because of the stratification the amplitudes of $\boldsymbol{B}_\perp$ and $\boldsymbol{v}_\perp$ depend on z. We can determine the general trends of these amplitudes by assuming that the Poynting flux

$$\boldsymbol{S} = \boldsymbol{E} \times \boldsymbol{B}/\mu_0 \tag{12}$$

is conserved[1]. Here $\boldsymbol{E} = -\boldsymbol{v} \times \boldsymbol{B}$ is the electric field. After using Eq. (9) to substitute $\boldsymbol{v}$ we find that $\boldsymbol{B}_\perp \propto \rho_0^{1/4}$, and it then trivially follows that $\boldsymbol{v}_\perp \propto \rho_0^{-1/4}$.

Since we want to be able to separate forward and backward propagating Alfvén waves in our simulations, it is useful to introduce the Elsasser vectors

$$\boldsymbol{Z}_\pm = \boldsymbol{v}_\perp \mp \frac{\boldsymbol{B}_\perp}{\sqrt{\mu_0 \rho}}, \tag{13}$$

which describe the forward and backward propagating Alfvén waves, respectively.

[1] Strictly speaking, the conserved quantity is the wave action e.g., Jacques (1977).

Table 1. Simulations of circularly polarised Alfvén waves in a stratified medium with density $\rho_0(0) = 5 \times 10^{-13}$ kg m^{-3} at the bottom of the grid. $\Delta t, N$ and L denote the time step measured in seconds, the number of grid points, and the length of the computational domain in scale heights, H, respectively. The vertical magnetic field, B_0, is given in T. $v_{\rm A0}$, β_0 and $\eta_0 = B_\perp/B_0$ are computed at $z = 0$.

Run	Δt (s)	N	$L\,(H)$	B_0 (T)	$v_{\rm A0}$(m s^{-1})	η_0	β_0
1a	0.0625	21 600	50	3×10^{-5}	3.8×10^4	0.007	23
1b	0.0625	21 600	50	3×10^{-5}	3.8×10^4	0.07	23
1c	0.0625	21 600	50	3×10^{-5}	3.8×10^4	0.7	23
2a	0.125	21 600	50	1.5×10^{-5}	1.8×10^4	0.007	82
2b	0.125	21 600	50	1.5×10^{-5}	1.8×10^4	0.07	82
2c	0.125	21 600	50	1.5×10^{-5}	1.8×10^4	0.7	82

3. Results

We use the one-dimensional code of Boynton & Torkelsson (1996) to simulate circularly polarised Alfvén waves in a stratified medium. The code solves Eqs. (1)–(3) in one spatial dimension. Table 1 describes the different models. $\Delta t, L$ and N denote the time step measured in seconds, the length of the computational domain and the number of grid points. The grid is sufficiently extended in all the runs so that the wave does not hit the upper boundary during the course of the simulation.

3.1. Basic properties of the propagation of an Alfvén wave

The temperature is taken to be 10^6 K in all Runs, which yields an isothermal sound speed of 1.29×10^5 m s^{-1}, and a scale height of 6.1×10^7 m. The temperature and density that we use are representative of the conditions in a coronal hole. In this medium we introduce a vertical magnetic field B_0, which gives an Alfvén velocity $v_{\rm A0} = B_0/\sqrt{\mu_0\rho_0(0)}$ at $z = 0$. It is often convenient to measure the strength of the magnetic field in terms of the plasma beta $\beta_0 = 2\mu_0 p/B_0^2$ at $z = 0$. The magnetic field that we use is weak compared to what we expect in the solar corona, however that is to some extent compensated for by the fact that the magnetic field is not expanding in the same way as in a real coronal hole because of the constraints that our geometry imposes on the magnetic field, and therefore we do reach realistic values of $\beta = 2\mu_0 p(z)/B_0^2$ in the upper part of our grid (Fig. 1) (because of the way in which β varies with z it is also difficult to study Alfvén waves with any lower β_0s, since they may produce cavitations further up). This also means that the Alfvén speed $v_{\rm A}$ increases with z, which has two kinds of consequences. Firstly the Alfvén wave is subsonic at the bottom of the corona, but it becomes supersonic at $z = 3.2$ H (Fig. 2a) and asymptotically approaches its maximal speed. Secondly, the wavelength increases in response to the increase of the Alfvén velocity. Eventually it can exceed the density scale height, H, but in none of our Runs does it exceed the Alfvén speed scale height, $H_{\rm A} = (1/v_{\rm A}\,{\rm d}v_{\rm A}/{\rm d}z)^{-1}$ (Fig. 2b).

This behaviour of the Alfvén velocity is an artefact of our simultaneous use of a plane-parallel geometry and a gravitational force that goes as $1/r^2$, as is appropriate for spherically symmetric models. In this way we avoid the problem that

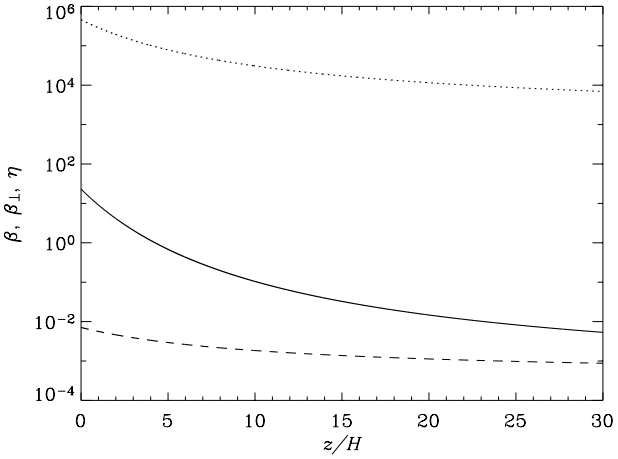

Fig. 1. $\beta = 2\mu_0 p/B_0^2$ (solid line), $\beta_\perp = 2\mu_0 p/B_\perp^2$ (dotted line) and the amplitude of the transverse Alfvén wave in terms of the background magnetic field $\eta = B_\perp/B_0$ (dashed line) versus z/H for Run 1a.

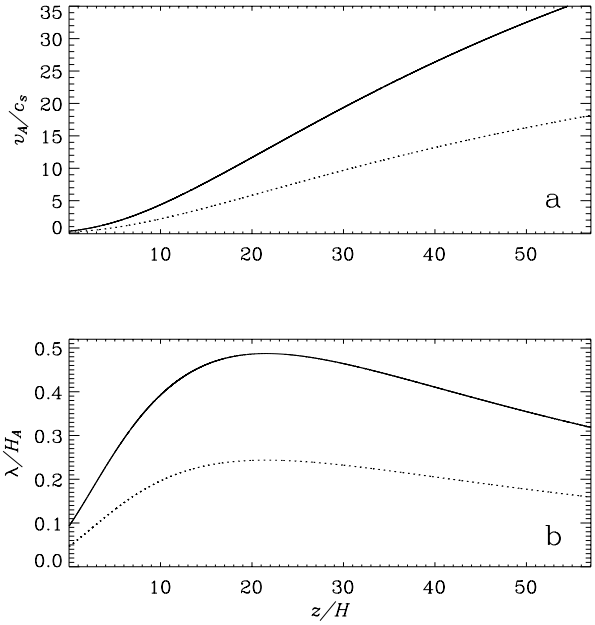

Fig. 2. a) Profile of Alfvén speed normalised to the sound speed in a stratified atmosphere versus z/H for Runs 1a–c (solid line) and Runs 2a–c (dotted line). **b**) The ratios of the wave length to the Alfvén speed scale height versus z/H for Runs 1a–c (solid line) and Runs 2a–c (dotted line).

An et al. (1989) encountered in that the Alfvén wave could reach infinity in a finite time and then be reflected. If we had properly taken into account the expansion of a spherically symmetric magnetic field, then the Alfvén speed would have had assumed its maximal value at a finite distance from the Sun. We consider this case in a forthcoming publication (Turkmani & Torkelsson, in preparation), but typically the maximum occurs a few solar radii (20–40 H) above the surface. In principle the Alfvén wave can be trapped in the region below the

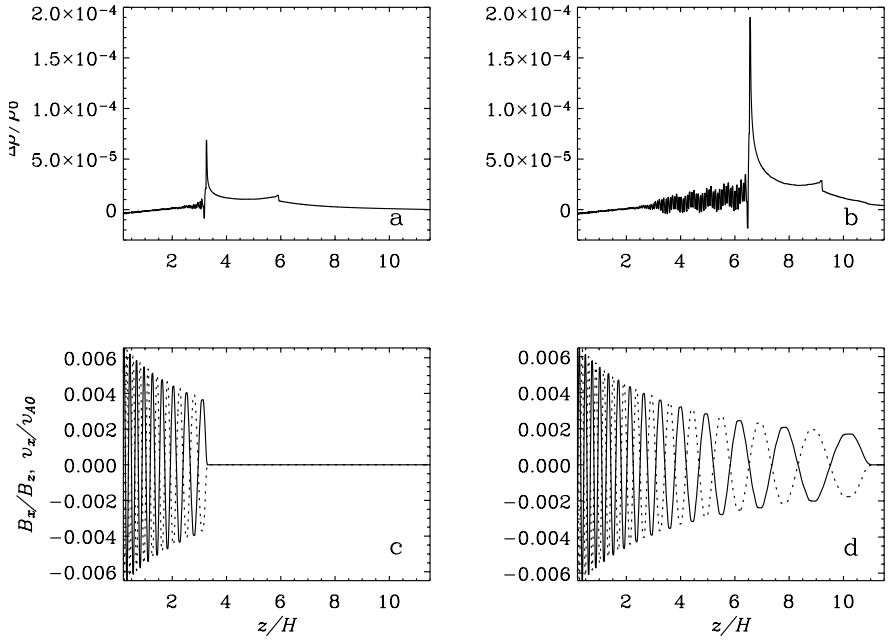

Fig. 3. Low amplitude magnetohydrodynamic waves propagating through a stratified medium (Run 1a). $\Delta\rho/\rho_0 = \frac{\rho-\rho_0}{\rho_0}$ versus z/H at **a**) $t/P = 9.4$ and **b**) $t/P = 14.6$. **c**) and **d**) B_x/B_z (solid line) and $v_x/v_{\rm A0}$ (dotted line) versus z/H at the same times.

maximum, but this effect is negligible at a temperature as high as 10^6 K (An et al. 1990).

The Alfvén wave is generated on the lower boundary by driving, B_x, B_y, v_x and v_y. The period of the Alfvén wave is usually $P = 300$ s, which is typical for the waves that are observed in the corona (e.g., De Moortel et al. 2002). $\eta_0 = (B_\perp/B_0)_0$ is the wave amplitude at $z = 0$, which corresponds to a velocity amplitude $\eta v_{\rm A0}$ at $z = 0$. The typical turbulent velocities of the corona vary between 20 and 50 km s^{-1} (e.g., Cheng et al. 1979; Zirker 1993), which is larger than the highest velocities at which we are driving the Alfvén wave, but due to the stratification the velocity amplitude increases with height in proportion to $\rho_0^{-1/4}$ as the density drops (Sect. 2). From a dynamical point of view it is more interesting to look at the variation of the amplitude of the fluctuating magnetic field, which varies as $\rho^{1/4}$. Consequently the magnetic pressure of the Alfvén wave decreases more slowly than the gas pressure. The Alfvén wave therefore gains dynamical importance as measured by $\beta_\perp = 2\mu_0 p/B_\perp^2$ (Fig. 1), though its relative amplitude decreases with z, which is different from the situation in the spherically symmetric problem, where the relative amplitude of the Alfvén wave starts to grow beyond a few solar radii. Therefore the role of nonlinear effects is underestimated in this paper.

3.2. Development of a density enhancement

We start by looking at the low amplitude Alfvén wave in Run 1a in Fig. 3. The Alfvén wave itself is represented by the x-components of the magnetic field and velocity in panels c) and d). These components show the expected anti-correlation, Eq. (9). Panel a) shows a density enhancement between $z = 3.2\ H$ and $6\ H$. It is originally created by the jump in magnetic pressure at the wave front. Its left edge moves together with the Alfvén wave front as long as the speed of the Alfvén wave front is smaller than $c_{\rm s} + v_z$, the speed of an acoustic perturbation, while the right edge always moves at the speed $c_{\rm s} + v_z$. In panels b) and d) the Alfvén wave front speed is larger than the sound speed, and consequently the Alfvén wave front overtakes the density peak.

The compressive effect of the Alfvén wave scales with η^2, and therefore the density enhancement, $\Delta\rho$ and v_z, becomes more pronounced in the high amplitude models. We see in Fig. 4a that the relative amplitude of the peak of the density enhancement of Run 1c reaches 0.68 at $t = 14.6P$. The corresponding increase in the outflow velocity, v_z, leads to that the Alfvén wave of Run 1c is faster than that of Run 1a (Fig. 4b), since the Alfvén wave propagates at the speed $v_{\rm A} + v_z$.

To demonstrate the effect of the magnetic pressure of the entire wave on the medium, we restarted Run 1c from $t_1 = 6.25P$ after having turned off B_x, B_y, v_x and v_y. We refer to this as the hydrodynamic (H) model, while the original model is referred to as the magnetic (M) model. The restarting time $t_1 = 6.25P$ is chosen so that the density enhancement is still ahead of the wave, and $v_{\rm A} < c_{\rm s}$ at the Alfvén wave front. We compare the density profiles of the two models in Fig. 5. In the H model, the left edge of the density enhancement travels with the speed $c_{\rm s} + v_z$ all the time, while in the M model it travels with the speed $v_{\rm A} + v_z$ before reaching the point where $v_{\rm A} = c_{\rm s}$ and with $c_{\rm s} + v_z$ thereafter. In addition to being more extended the density enhancement of the M model attains a higher amplitude also. This shows how the magnetic pressure continuously adds energy to the density enhancement. On the other hand the

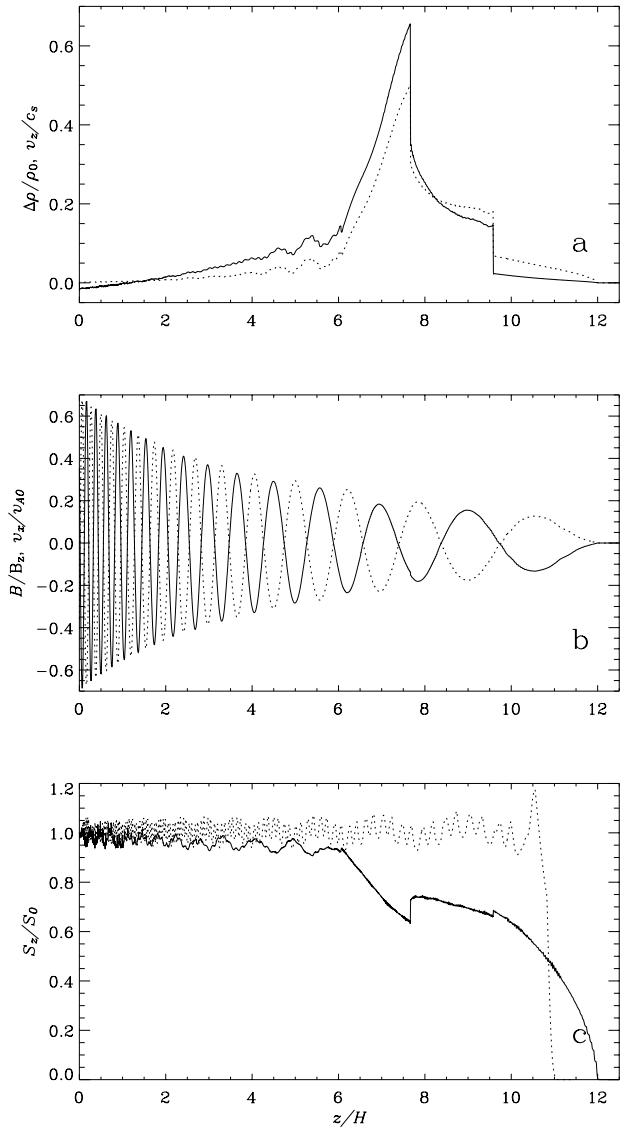

Fig. 4. High amplitude magnetohydrodynamic waves in a stratified medium (Run 1c) at $t/P = 14.6$ plotted as functions of z/H. **a**) $\Delta\rho/\rho_0$ (solid line) and v_z/c_s (dotted line), **b**) B_x/B_z and v_x/v_{A0}, and **c**) the Poynting flux S_z/S_0 for Run 1c (solid line) compared to that of the low amplitude Run 1a (dotted line) at the same time. S_0 is the Poynting flux at $z = 0$.

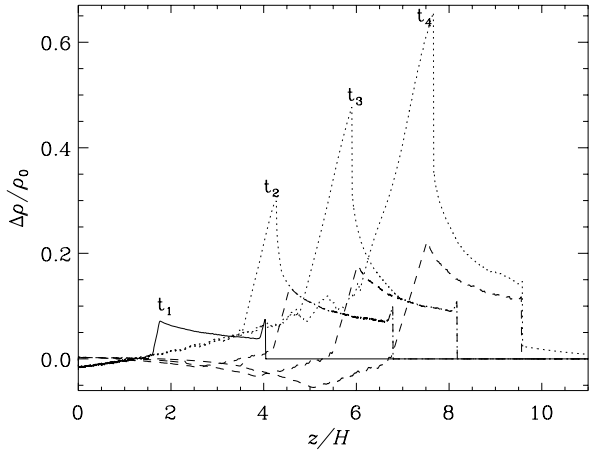

Fig. 5. $\Delta\rho/\rho_0$ versus z/H for Run 1c. The solid line represents $\Delta\rho/\rho_0$ at $t_1 = 6.25P$, the dotted and the dashed lines represent $\Delta\rho/\rho_0$ for the M and H models respectively, at $t_2 = 10.4P$, $t_3 = 12.5P$ and $t_4 = 14.6P$.

gradual growth of $\Delta\rho/\rho$ that we see in the H model is the result of the stratification only.

The significance of the work done by the wave is shown most clearly at times t_3 and t_4 (Fig. 5). At t_3 the Alfvén wave has reached $z = 7\,H$, and we see that the density profiles start to diverge at this point. The difference between the H and M models grows as the wave overtakes the density enhancement and continues to do work on the medium. Behind the density enhancement, we find a region with a mass deficit in the H model, while this region is continuously re-filled with matter in the M model.

3.3. Wave reflection and parametric decay

3.3.1. Low amplitude waves

To trace the wave reflection, we use the Elsasser vectors introduced in Eq. (13). Figure 6 shows the x- and y-components of the two Elsasser vectors, $\boldsymbol{Z}_\pm$, for the low amplitude Run 1a ($\eta = 0.007$). We get similar results for Run 1b. The forward-propagating wave is left-circularly polarised since the y-component is leading, but the reflected wave is right-circularly polarised since the x-component is leading. The relative amplitude of the reflected wave is $\frac{|Z_-|}{|Z_+|} \approx 0.04$, but the x-component of $\boldsymbol{Z}_-$ is mostly negative. To trace the effect of the reflected wave on the mother wave we compare the amplitude of $\boldsymbol{Z}_+$ to its theoretical value (Fig. 6a dashed line).

3.3.2. High amplitude waves

Figure 7 shows the two Elsasser vectors for the high amplitude Run 1c ($\eta = 0.7$). In Fig. 7a we see a significant loss of the amplitude of $\boldsymbol{Z}_+$ compared to the simple scaling relation (Sect. 2). As in model 1a a small amplitude backward propagating Alfvén wave is generated at $z > 13\,H$, but in addition the density enhancement at $z = 10\,H$ acts like a new source for $\boldsymbol{Z}_-$. The reflected wave reaches $\frac{|Z_-|}{|Z_+|} \approx 0.15$ in the density enhancement, but its wave length is significantly shorter there than in front of the density enhancement, and it appears to not be circularly polarised.

The small amplitude density oscillation that can be seen to the left of the peak of $\Delta\rho/\rho_0$ in Fig. 4a at $t/P = 14.6$ has grown significantly in amplitude at the later time $t/P = 17.5$ (Fig. 7). The simultaneous appearance of a density wave and a backward propagating magnetic wave is the signature of the parametric decay of the original Alfvén wave. We notice that the parametric decay does not become pronounced until the density enhancement in Run 1c reaches $z/H \sim 6$–10 where $\beta \sim 0.42$–0.1.

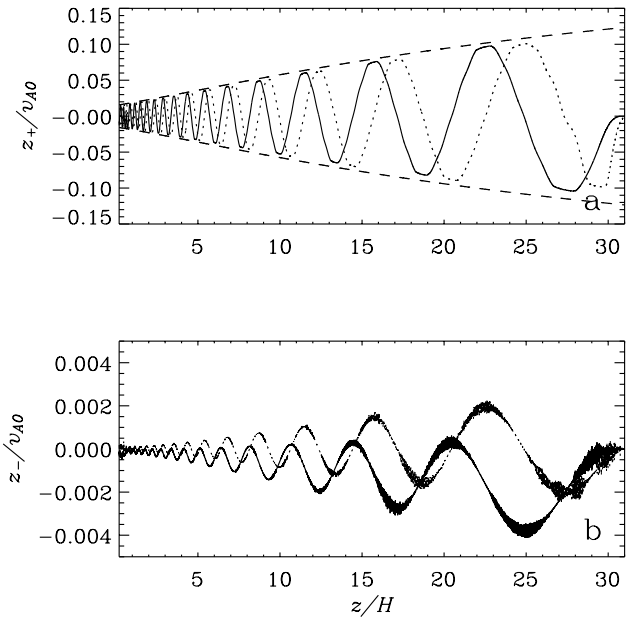

Fig. 6. The two Elsasser vectors for Run 1a at $t/P = 17.7$ (x-components: solid lines; y-components: dotted lines). **a**) $\mathbf{Z}_+/v_{A0}$ versus z/H, and $\pm\frac{1}{\eta}$ (dashed lines). **b** $\mathbf{Z}_-/v_{A0}$ versus z/H. Note the difference in scale between the two panels.

3.4. Energetics

In Fig. 8 we plot the time averages of the work and Poynting flux over a wave period (between $t/P = 13.6$ and 14.6) for Runs 1a and 1c. In the low amplitude Run, there is very little work done, which is demonstrated by the flat profile of the Poynting flux. For the high amplitude Run there is a considerable loss of Poynting flux above $z = 5.5\,H$. Most of the energy is spent as mechanical work done by the Alfvén wave on the medium. An interesting feature is that the gradual damping of the Poynting flux between $z/H = 6$ and 8 at $t/P = 14.6$ coincides with the smooth rise of the density enhancement (Fig. 4).

3.5. Higher beta models

Runs 2a–c have the same characteristics as Runs 1a–c except that the magnetic field is 50% weaker. The reflection off the background density stratification is of the order of $\frac{|Z_-|}{|Z_+|} \approx 0.022$ for all these Runs. The high amplitude Run 2c generates a density enhancement similar to that of Run 1c, but its amplitude is merely half of that of Run 1c. The relative amplitude of the backward propagating wave that it is generating is also reduced by 50%.

4. Discussion

The general aim of our work is to study the properties of propagating circularly polarised Alfvén waves in a stratified medium. Because of the limitations of our model, and the limited part of parameter space that can be explored with our numerical code, our results should not be taken literally; they are only

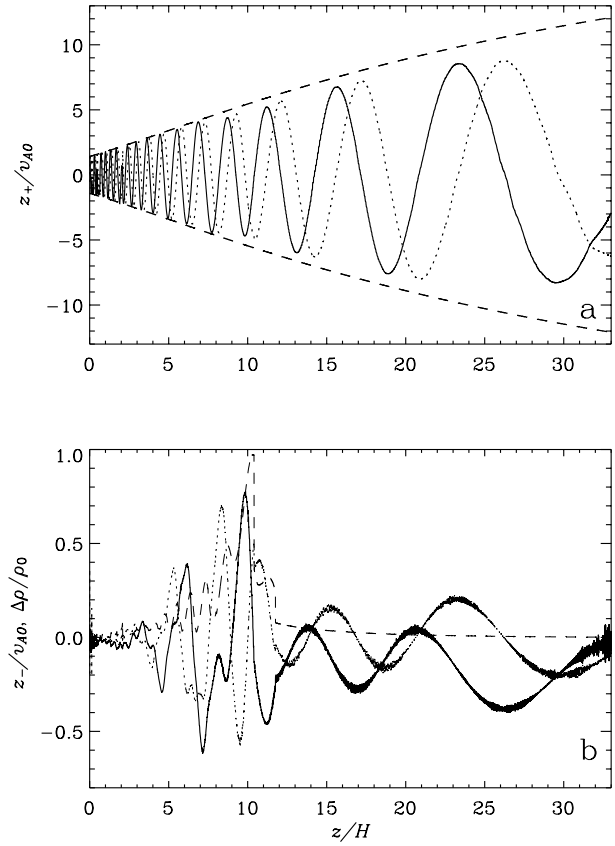

Fig. 7. The two Elsasser vectors for Run 1c at $t/P = 17.5$ (x-components: solid lines; y-components: dotted lines). **a**) $\mathbf{Z}_+/v_{A0}$ versus z/H (solid line), and $\pm\frac{1}{\eta}$ (dashed line). **b**) $\mathbf{Z}_-/v_{A0}$ versus z/H (solid line) and $\Delta\rho/\rho_0$ (dashed line) at the same time. Note the difference in scale between the two panels.

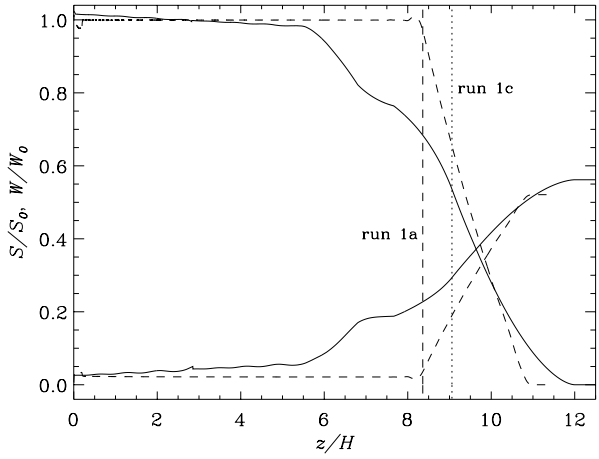

Fig. 8. The time average of the Poynting flux (*top left*) and the integrated work the Alfvén wave performs on the medium via the Lorentz force (*bottom left*) during one period of the Alfvén wave. Solid lines are for the high amplitude Run 1c and dashed lines for the low amplitude Run 1a. The curves have been scaled by the Poynting flux at $z = 0$. The vertical lines indicate the positions of the Alfvén wave fronts at the start of the averaging at $t/P = 13.6$.

indicative of general trends. In a previous paper (Turkmani & Torkelsson 2003) we studied the dynamics of circularly polarised Alfvén waves in a homogeneous medium, and thus by comparing these two papers we can learn about the effect of the stratification on the Alfvén waves, and in a future paper (Turkmani & Torkelsson in preparation) we will go from the plane-parallel geometry to the spherically symmetric case, which will then reveal the effect of the geometrical expansion on the waves.

Circularly polarised waves are much more weakly damped than linearly polarised waves. When we compare our Figs. 8 with 9 of Boynton & Torkelsson (1996) we notice that the linearly polarised wave loses most of its energy below $z = 0.4\,R_\odot$, whereas the circularly polarised wave starts to lose significant amounts of energy only above $z = 5\,H = 0.4\,R_\odot$. This makes circularly polarised waves better at transferring energy from the lower corona to the outer corona and solar wind.

There are two important ways in which a circularly polarised Alfvén wave can lose energy, through reflection and through a parametric decay into a density wave and a backward propagating Alfvén wave. While the reflection is a linear process that depends on the Alfvén speed profile, the parametric decay is a nonlinear process, whose importance increases with the amplitude of the wave. This makes it possible to disentangle the two processes by comparing the results for different amplitudes of the Alfvén wave. The reflection can depend on the strength of the background magnetic field though, and in the parameter range that we have studied the relative amplitude of the reflected wave is proportional to the strength of the magnetic field. It is worth noticing that we do not find the total reflection of the Alfvén wave that was predicted by An et al. (1989). The reason for this is that we do not assume the exponential stratification that they assumed. With our weaker stratification it takes an infinite amount of time for the Alfvén wave to reach infinity, and thus the wave cannot be reflected at infinity.

In the homogeneous models we noticed that the parametric decay of a circularly polarised Alfvén wave takes place only in low beta models. Consistent with this we find that in the stratified models, the decay does not become noticeable until the density enhancement reaches a region where $\beta < 0.4$. In the homogeneous models the decay can be observed for a wave with an amplitude as small as $\eta = 0.07$, but in the stratified models the initial amplitude must be as high as $\eta = 0.7$, because the amplitude of the wave depends on ρ, and a wave of a lower amplitude at $z = 0$ will be too weak when it reaches the region, in which β is small enough for the parametric decay to set in.

Acknowledgements. This research was sponsored by the Swedish Research Council and by the European Commission under research training network HPRN-CT-2001-00310. R.T. wants to thank the solar MHD group at the University of St. Andrews for hospitality during part of this work. We thank an anonymous referee for comments that have helped to improve the paper.

References

Alfvén, H., & Fälthammar, C.-G. 1963, Cosmical electrodynamics, Fundamental principles (Oxford: Clarendon Press)
An, C.-H., Musielak, Z. E., Moore, R. L., & Suess, S. T., 1989, ApJ, 345, 597
An, C.-H., Suess, S. T., Moore, R. L., Musielak, Z. E. 1990, ApJ, 350, 309
Belcher, J. W., & Davis, L. 1971, JGR, 79, 4174
Biermann, L. 1948, Z. Astrophys., 25, 161
Boynton, G. C., & Torkelsson, U. 1996, A&A, 308, 299
Cheng, C.-C., Doschek, G. A., & Feldman, U. 1979, ApJ, 227, 1037
Cohen, R. H., & Kulsrud, R. M. 1974, Phys. Fluids, 17, 2215
De Moortel, I., & Hood, A. W. 2004, A&A, 415, 705
De Moortel, I., Ireland, J., Hood, A. W., & Walsh, R. W. 2002, A&A, 387, L13
Del Zanna, L., Velli, M., & Londrillo, P. 2001, A&A, 367, 705
Ferraro, V. C. A. 1954, ApJ, 119, 393
Galeev, A. A., & Oraevskii, V. N. 1963, Sov. Phys. Dokl., 7, 988
Jacques, S. A. 1977, ApJ, 215, 942
Leer, E., Holzer, T. E., & Flå, T. 1982, Space Sci. Rev., 33, 161
Leroy, B. 1980, A&A, 91, 136
Lou, Y., & Rosner, R. 1994, ApJ, 424, 429
Nakariakov, V. M., Ofman, L., & Arber, T. D. 2000, A&A, 353, 741
Ofman, L., & Davila, J. M. 1997, ApJ, 476, 357
Oughton, S., Matthaeus, W. H., Dmitruk, P., et al. 2001, ApJ, 551, 565
Sheeley, N. R., Jr., Wang, Y.-M., Hawley, S. H., et al. 1997, ApJ, 484, 472
Sagdeev, R. Z., & Galeev, A. A. 1969, Nonlinear Plasma Theory, (New York: Benjamin)
Turkmani, R., & Torkelsson, U. 2003, A&A, 409, 813
Zirker, J. B. 1993, Sol. Phys., 148, 43